Numerical and Experimental Investigation for Stability Lobes Prediction in Thin Wall Machining

O. B. Adetoro, P. H. Wen, W. M. Sim, R. Vepa

Abstract— **A Finite Element Analysis (FEA) and Fourier transform approach to obtain frequency response function (FRF) is presented in this paper. The aim in this paper is to eliminate the need for the classical impact experimental approach used in extracting structure's FRF.**

The numerical and experimental FRFs have been used to obtain stable regions in machining of thin walled structures, which gives a good comparison. Examples are presented and compared with experimental results with a satisfactory agreement.

Index Terms— **FEA, frequency response function, discrete Fourier transform, stability lobes, transfer function.**

I. INTRODUCTION

Even after such an extensive research into chatter vibration, it still is (as stated by Taylor just over a century ago) one of the most obscure and delicate of all problems facing the machinist [1]. It certainly undermines and reduces productivity and surface quality in manufacturing. It could also increase the cost through possible machine or tool damage. It is because of these effects that it has been the topic of several studies over the years. The stability lobes/chart approach is more practical from the stance of a machinist, while its extraction can be somewhat tedious. The accuracy of the predicted stable region relies on the transfer function identified at the cutter-workpiece contact zone. The classical approach to obtaining the transfer function is through impact test. However, this paper proposes an alternative approach which uses finite element method (FEM) modal analysis to obtain the transfer function at specified cutter-workpiece contact zones.

While the transfer functions for the tool can be assumed to be constant, the workpiece transfer function/dynamics are constantly changing as material is removed. Moreover, in thin wall machining, the workpiece vibration is significant compared to that of the tool. Hence the transfer function used must be precise. It will be highly impractical to perform impact tests at multiple stages of machining, hence the need for an offline approach to stability lobes prediction.

The prediction of stable conditions in the form of charts started when, Tobias [2] and Tlusty [3] simultaneously made the remarkable discovery that the most important sources of self-excitation, regeneration and mode coupling were associated with the structural dynamics of the machine tool-workpiece system and the feedback response between subsequent cuts. At this early stage, the stability lobes approach that is widely used by researches to predict the stable margin was also established by [2]. While Tlusty and Polacek [3] obtained an expression for chatter free axial depth of cut using the cutting force coefficient, and the real part of the structure's transfer function in the direction normal to the machined surface. This was later improved by Tlusty [4] to include the effect of the spindle speed on the chatter frequency ('lobbing effect'). Other studies on the stability of metal cutting were reported Merritt [5].

Though, a pioneering research, the stability models by Tobias and Tlusty are only applicable to orthogonal metal cutting where the directional dynamic milling coefficients are constant and not periodic. This is quite the contrary in milling due to the rotating cuter with multiple teeth. In order to accommodate this directional dynamic milling coefficients, time domain simulation of the milling process was introduced by Tlusty [6, 7]. Slavicek [8] and Vanherck [9] made the assumption that all the cutter teeth have a constant directional orientation in their study of the effect of irregular pitch on the stability. Sridhar et al. [10, 11] and Hohn [12] later carried out an in-depth study in which, they introduced time-varying directional coefficients in their chatter stability analysis. They used the system's state transition matrix in their stability model, which helps to eliminate the periodic and time delay terms. Optiz et al. [13, 14] used an average value of the periodic directional coefficients in the analysis. Tlusty [15] made an attempt to apply the orthogonal model to milling process by assuming the teeth of the tool had equal pitch, was simultaneously in cut and that the motion was rectilinear with constant depth of cut. The Nyquist criterion was used by Minis and Yanushevsky [16, 17] and Lee et al. [18, 19] to obtain the stability limits. Lee et al. used the mean value method to replace the time varying directional coefficients by a constant. Up until this point there existed no proposed analytical approach to predicting the stability

Manuscript received March 18, 2009. This work was supported in part by EPSRC and Airbus UK under Grant BS123456.

O. B. Adetoro is with Queen Mary University of London, Queen Mary, University of London, Mile End Road, London E1 4NS, UK (e-mail: o.adetoro@qmul.ac.uk).

*P. H. Wen is with Queen Mary University of London, Queen Mary, University of London, Mile End Road, London E1 4NS, UK; (phone: 44(0)20-7882-5371, fax: 44(0)20-8983-1007; email: p.h.wen@qmul.ac.uk).

W. M. Sim is with Airbus, New Filton House, Golf Course Lane, Filton BS34 7AR, UK (e-mail: WeiMing.Sim@airbus.com).

R. Vepa is with Queen Mary University of London, Queen Mary, University of London, Mile End Road, London E1 4NS, UK (e-mail: r.vepa@qmul.ac.uk).

margin for milling, whilst respecting the varying directional dynamic milling coefficients.

Following the in-depth work by Budak, [20], Altintas and Budak [21, 22, 23] later proposed an analytic approach in which the zeroth order term in the Fourier series expansion (single frequency solution or zeroth order approximation) of the time varying coefficients was adopted. A similar model was later used by Altintas et al. [24], where they proposed an average scheme of the immersion angle, while the analytical model was later extended to include three directions by Altintas [25], where the axial immersion angle was also assumed to be constant. Campa et al. [26] later proposed an averaging approach to calculating the axial immersion angle in order to solve the stability model analytically. Adetoro et al. [27] recently proposed some modifications to the stability lobe model by Altintas [25]. The modifications allow for the inclusion of the nonlinear nature of the cutting force coefficients and the axial immersion angle along the axial depth of cut in the prediction of more accurate stable cutting conditions. The results were obtained using a numerical approach

To analytically predict the stable region the dynamic parameters identified at the cutter-workpiece contact zone are used. The classical approach to obtaining the dynamic parameters is through impact tests. Unlike in tool chatter, the dynamic parameters are not constant along the workpiece and are constantly changing as material is removed and the geometry changes. Attempts were made by Thevenot [28] to use this varying dynamics in thin wall machining to initiate the variation of the spindle speed along the workpiece in order to improve surface finish. The tendency in this approach however is the tendency for new marks to be left on the surface due to the change in cutting conditions as seen from their experimental results. Budak considered the variations the dynamics of the cutter and the workpiece along the axial direction [22, 23]. Seguy et al. [29] just recently carried out a study to include the varying dynamics along a thin wall and thin floor section, although the results show certain discrepancies which could have arisen from the assumptions made. It is however clear in thin wall that it is insufficient to assume the dynamics of the workpiece are constant, which has previously been the case.

This paper presents a numerical approach to obtaining the structures transfer function, which is required in the stability model. This approach aims to eliminate the need for series of experimental impact testing at various points on a thin walled workpiece in order to obtain the corresponding transfer function at the point. The only experimental result required would be the one to obtain the damping parameters of the structure, which can also be eliminated by adapting the approach to predicting the damping parameters by Adetoro et al. [35, 36]. However to obtain the varying dynamics along the tool-path, this approach can be used to prevent further experimental impact testing. The full transfer function matrix in all the three translational directions can also be easily extracted. Compared to experimental methods, this can prove difficult in certain translational directions. The approach is presented here with the 2-D stability model in [21] and can easily be adapted to the 3-D model in [25, 27] as shown by Adetoro t al. [30].

II. Chatter Stability Model

The stability model used in this paper is the model proposed by Altintas and Budak [21] as summarized below. The periodic milling forces excite the cutter and the workpiece causing two orthogonal dynamic displacements x and y in the global axis.

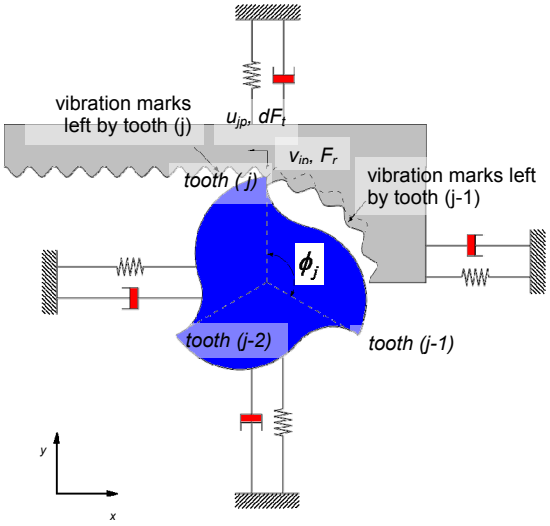

Figure 1 – Dynamic Milling Model.

This generates undulations on the machined surface and each tooth removes the undulations generated by the previous tooth (Figure 1). Therefore leading to a modulated chip thickness which can be expressed as

$$h_j(\phi) = s_t \sin\phi_j + \left(\upsilon_{jc}^0 - \upsilon_{jw}^0\right) - \left(\upsilon_{jc} - \upsilon_{jw}\right), \tag{1}$$

where s_t is the feed per tooth, $\left(\upsilon_{jc}^0, \upsilon_{jc}\right)$ and $\left(\upsilon_{jw}^0, \upsilon_{jw}\right)$ are the dynamic displacement of the cutter and workpiece at the previous and present tooth periods respectively, $\phi_j = (j-1)\phi_p + \Omega t$ is the angular immersion of tooth j for a cutter (Ω is the angular speed), with constant pitch angle $\phi_p = 2\pi/N$ (N is the number of teeth).

The dynamic displacements in the chip thickness direction due to tool and workpiece vibrations are defined as

$$\upsilon_{jp} = -x_p \sin\phi_j - y_p \cos\phi_j \quad (p = c, w), \tag{2}$$

where c and w indicate the cutter and workpiece respectively, x_p, y_p and x_p^0, y_p^0 are the dynamic displacements in the global axis for the current and previous tooth periods respectively.

By eliminating the static part in (1), the dynamic chip thickness in milling is defined as

$$h_j(\phi) = \Delta x \sin\phi_j - \Delta y \cos\phi_j, \tag{3}$$

where,

$$\begin{aligned} \Delta x &= \left(x_c - x_c^0\right) - \left(x_w - x_w^0\right), \\ \Delta y &= \left(y_c - y_c^0\right) - \left(y_w - y_w^0\right), \end{aligned} \tag{4}$$

Therefore, the dynamic forces on tooth j (using ‘‘Exponential Force Coefficient Model’’, [20]) in the tangential and radial directions can be defined as

$$F_{tj}(\phi) = K_t a h_j(\phi),$$
$$F_{rj}(\phi) = K_r F_{tj}(\phi), \quad (5)$$

where a is the axial depth of cut (ADOC), and K_t and K_r are the tangential and radial cutting force coefficients respectively.

For simplicity, like in other studies these cutting force coefficients have been taken as constant here. However they have been shown to affect the predicted margin by Adetoro et al. [27]. This approach here can easily be adapted to the modifications they proposed. Therefore, by substituting (3) into (5) and resolving in the global directions, the following expression is obtained

$$\begin{Bmatrix} F_x \\ F_y \end{Bmatrix} = \frac{1}{2} a K_t \begin{bmatrix} a_{xx} & a_{xy} \\ a_{yx} & a_{yy} \end{bmatrix} \begin{Bmatrix} \Delta x \\ \Delta y \end{Bmatrix}, \quad (6)$$

where a_{xy} are the periodic directional cutting coefficients and depends on the angular position of the cutter and the radial cutting force coefficient K_r, thereby making (6) a function of time

$$\{F(t)\} = \frac{1}{2} a K_t [A(t)] \{\Delta(t)\}, \quad (7)$$

As mentioned in previous section, $[A(t)]$ is periodic at the tooth passing frequency $\omega = N\Omega$, therefore its Fourier series expansion is used for the solution of the system. The average value in the Fourier series expansion (single frequency solution) of the time varying directional coefficients is used in this paper. Hence, (7) reduces to

$$\{F(t)\} = \frac{1}{2} a K_t [A_0] \{\Delta(t)\}, \quad (8)$$

where $[A_0]$ is the time invariant, but radial immersion dependent directional cutting coefficient matrix.

From the frequency response function FRF and the dynamic forces, the dynamic displacement vector in (8) can be solved. Using the response at present time (t) and the previous tooth period $(T-t)$, equation (8) can be expressed as [21]

$$\{F\} e^{i\omega_c t} = \frac{1}{2} a K_t [A_0] (1 - e^{-i\omega_c T}) [G(i\omega_c)] \{F\} e^{i\omega_c t}, \quad (9)$$

where $\{F\}$ represents the amplitude of the dynamic cutting force $\{F(t)\}$, $[G(i\omega_c)]$ is the transfer function matrix.

The transfer function matrix $[G(i\omega_c)]$ is the main focus of this paper. It is defined as

$$[G(i\omega_c)] = [G_c(i\omega_c)] + [G_w(i\omega_c)], \quad (10)$$

where

$$[G_p(i\omega_c)] = \begin{bmatrix} G_{p_{xx}}(i\omega_c) & G_{p_{xy}}(i\omega_c) \\ G_{p_{yx}}(i\omega_c) & G_{p_{yy}}(i\omega_c) \end{bmatrix}, \ (p = c, w) \quad (11)$$

Equation (9) has a non-trivial solution only if its determinant is zero,

$$\det[[I] + \Lambda[G_0(i\omega_c)]] = 0, \quad (12)$$

where $[G_0] = [A_0][G]$

The eigenvalues is defined as

$$\Lambda = -\frac{N}{4\pi} K_t a (1 - e^{-i\omega T}), \quad (13)$$

Solving (12) numerically will give eigenvalues with complex and real parts $(\Lambda = \Lambda_R + i\Lambda_I)$, and from Euler's formula, $e^{-i\omega_c T} = \cos\omega_c T - i \sin\omega_c T$. When this is substituted into (13), the complex part has to vanish (i.e. $\Lambda_I (1 - \cos\omega_c T) = \Lambda_R \sin\omega_c T$) because the axial depth of cut a is a real value. Therefore,

$$\kappa = \frac{\Lambda_I}{\Lambda_R} = \frac{\sin\omega_c T}{1 - \cos\omega_c T} = \tan\psi, \quad (14)$$

where ψ is the phase shift of the eigenvalues. From this expression the relationship between the frequency and the spindle speed is [21] obtained

$$\omega_c T = \varepsilon + 2k\pi,$$
$$\varepsilon = \pi - 2\psi,$$
$$\psi = \tan^{-1}\kappa, \quad (15)$$
$$n = \frac{60}{NT},$$

where ε is the phase difference between the inner and outer undulations, k is an integer corresponding to the number of vibration waves within a tooth period and n is the spindle speed (rpm).

Substituting (14) into (13) and the final expression for chatter free axial depth of cut becomes

$$a_{\lim} = -\frac{2\pi\Lambda_R}{NK_t}(1 + \kappa^2) \quad (16)$$

Therefore for a given chatter frequency, ω_c the eigenvalues are obtained from (12), which allows for the critical depth of cut to be calculated using (16) and finally the spindle speed using (15) for different number of vibration waves, k. This is repeated for various frequencies around the structures dominant modes.

III. The System's Transfer Function

To obtain the transfer function of the system, the modal dynamic analysis on Abaqus was used. Being a very well developed model, the modal dynamic analysis gives the response of a defined domain as a function of time for a given time dependent loading. This gives the linear response of the structure, which can be very easily extracted once the modes of the system are available. This is due to the modes being orthogonal, thereby rendering the system as a mere combination of single degree of freedom systems. The modes are extracted in a frequency extraction analysis, which utilizes the Lanczos algorithm. The free vibration solution of the equation of motion takes the form

$$\{x\} = \{X\} \sin\omega t \quad (17)$$

When substituted into equation of motion, an eigenvalue problem is obtained as

$$\left(\left[K\right]-\omega^2\left[M\right]\right)\left\{X\right\}=0, \tag{18}$$

where $\left[K\right]$ is the stiffness matrix of the system, $\left[M\right]$ is the mass matrix, ω_n^2 is the eigenvalue or in this case the undamped natural frequency of the system squared and $\left\{X\right\}$ is the eigenvector (the mode of vibration or mode shape).

The transient modal dynamic analysis on Abaqus was used to solve the eigenvalue problem and to predict the system's transfer function. The modal dynamic analysis gives the response of a defined domain as a function of time for a given time dependent loading. The response obtained is the linear response of the structure, which is easily extracted once the modes of the system are available. The modes are extracted in a frequency extraction analysis, which utilizes the Lanczos algorithm due to the size of the eigenproblem in equation (4.9). The algorithm is detailed by Grimes et al. [31] and in the Abaqus user manual [32]. Therefore, when the model is projected onto the eigenmodes used for the system's dynamic representation (i.e. uncoupling the system's stiffness, mass and damping matrices using the orthogonality property explained earlier), its equation of motion is uncoupled and an expression at time t is [32] obtained

$$\ddot{q}_p+2\zeta_p\omega_{n,p}q_p+\omega_{n,p}^2q_p=f_{t-\Delta t}+\frac{\Delta f}{\Delta t}\Delta t, \tag{19}$$

where p is the mode number, q_p is the amplitude of the response of mode p (in the ''generalized coordinate''), $\omega_{n,p}$ is the undamped natural frequency of mode p, Δf is the change in f over the time increment, Δt assuming the excitation varies linearly within each increment and ζ_p is the damping ratio for mode p.

The solutions is obtained [32] in the form

$$\begin{Bmatrix} q_{t+\Delta t} \\ \dot{q}_{t+\Delta t} \end{Bmatrix}=\begin{bmatrix} d_{11} & d_{12} \\ d_{21} & d_{22} \end{bmatrix}\begin{Bmatrix} q_t \\ \dot{q}_t \end{Bmatrix}+\begin{bmatrix} e_{11} & e_{12} \\ e_{21} & e_{22} \end{bmatrix}\begin{Bmatrix} f_t \\ f_{t+\Delta t} \end{Bmatrix}, \tag{20}$$

where $i,l=1,2$, d_{il} and e_{il} are constants, which are dependent on the three different cases of non-rigid body motion.

These cases are based on the oscillation modes - underdamped, critical damping and overdamped. These constants are detailed in Abaqus user manual [32]. For the underdamped case, the constants are given as follows [32]

$$a_{11}=\exp\left(-\zeta\omega_n\Delta t\right)\left(\frac{\zeta\omega_n}{\overline{\omega}}\sin\overline{\omega}\Delta t+\cos\overline{\omega}\Delta t\right) \tag{21a}$$

$$a_{12}=\exp\left(-\zeta\omega_n\Delta t\right)\frac{1}{\overline{\omega}}\sin\overline{\omega}\Delta t, \tag{21b}$$

$$a_{21}=-\exp\left(-\zeta\omega_n\Delta t\right)\frac{\omega}{\sqrt{1-\zeta^2}}\sin\overline{\omega}\Delta t, \tag{21c}$$

$$a_{22}=\exp\left(-\zeta\omega_n\Delta t\right)\left(\cos\overline{\omega}\Delta t-\frac{\zeta\omega_n}{\overline{\omega}}\sin\overline{\omega}\Delta t\right), \tag{21d}$$

$$b_{11}=-\exp\left(-\zeta\omega_n\Delta t\right)\left[\left(\frac{\zeta}{\omega_n\overline{\omega}}+\frac{2\zeta^2-1}{\omega_n^2\overline{\omega}\Delta t}\right)\sin\overline{\omega}\Delta t+\left(\frac{1}{\omega_n^2}+\frac{2\zeta}{\omega_n^3\Delta t}\right)\cos\overline{\omega}\Delta t\right]+\frac{2\zeta}{\omega_n^3\Delta t}, \tag{22a}$$

$$b_{12}=\left[\left(\frac{2\zeta^2-1}{\omega_n^2\overline{\omega}\Delta t}\right)\sin\overline{\omega}\Delta t+\left(\frac{2\zeta}{\omega_n^3\Delta t}\right)\cos\overline{\omega}\Delta t\right]\times\exp\left(-\zeta\omega_n\Delta t\right)+\frac{1}{\omega_n^2}-\frac{2\zeta}{\omega_n^3\Delta t}, \tag{22b}$$

$$b_{21}=\left[\left(\frac{1}{\omega_n^2}+\frac{2\zeta}{\omega_n^3\Delta t}\right)\left(\overline{\omega}\sin\overline{\omega}\Delta t+\zeta\omega_n\cos\overline{\omega}\Delta t\right)-\left(\frac{2\zeta^2-1}{\omega_n^2\overline{\omega}\Delta t}+\frac{\zeta}{\omega\Delta t}\right)\left(\overline{\omega}\cos\overline{\omega}\Delta t-\zeta\omega_n\sin\overline{\omega}\Delta t\right)\right]\times\exp\left(-\zeta\omega_n\Delta t\right)-\frac{1}{\omega_n^2\Delta t}, \tag{22c}$$

$$b_{22}=\left[-\left(\frac{2\zeta^2-1}{\omega_n^2\overline{\omega}\Delta t}\right)\left(\zeta\omega_n\sin\overline{\omega}\Delta t-\overline{\omega}\cos\overline{\omega}\Delta t\right)-\left(\frac{2\zeta}{\omega_n^3\Delta t}\right)\left(\overline{\omega}\sin\overline{\omega}\Delta t+\zeta\omega_n\cos\overline{\omega}\Delta t\right)\right]\times\exp\left(-\zeta\omega_n\Delta t\right)+\frac{1}{\omega_n^2\Delta t}, \tag{22d}$$

Since the time integrations is done in generalized coordinates, the response of the physical variables are obtained through summation

$$u=\sum_p^N X_pq_p, \tag{23}$$

where X_p are the eigenvector corresponding to the mode p and u is the actual nodal displacement. From this the velocity and hence the nodal acceleration can be derived.

The system's frequency response function (FRF), is simply the ratio of the Fourier transform of the output over the input (in the case of a system with single input and output).

$$G_{p_{nn}}\left(\omega\right)=\frac{X_{p_{nn}}\left(\omega\right)}{F_{p_{nn}}\left(\omega\right)}\ \left(p=c,w\right),\left(n=x,y\right) \tag{24}$$

The discrete Fourier transform algorithm is adopted, which is defined [33] as

$$\begin{aligned}\mathrm{Re}\,H\left[k\right]&=\sum_{i=0}^{M-1}h\left[i\right]\cos\left(\frac{2\pi kt}{M}\right),\\ \mathrm{Im}\,H\left[k\right]&=-\sum_{i=0}^{M-1}h\left[i\right]\sin\left(\frac{2\pi kt}{M}\right),\end{aligned} \tag{25}$$

where k runs from 0 to $M/2$, $\mathrm{Re}\,H[k]$ and $\mathrm{Im}\,H[k]$ are the real and imaginary parts of the frequency domain signal and $h[i]$ is the time domain signal.

The corresponding frequencies are defined as

$$\omega = \frac{k \cdot f}{M-1}, \tag{26}$$

were ω is the frequency, f is the sampling frequency.

IV. The Finite Element Model

The workpiece material used in the FEM model is Aluminium Alloy 7010 T7651. The material properties required for generating the stiffness and mass matrices are: Density - 2.823×10^{3} Kg m^{-3}, Young's Modulus - 69.809 GPa and Poisson Ratio - 0.337. Three different types of workpiece were used in the finite element analysis (FEA). The dimensions are shown in Figure 2 and the different thicknesses, (W) are shown in tables 1, 2 and 3 respectively.

The assumptions made in the finite element analysis (FEA) are as follows:

1) The workpiece was bolted at the back surface during the impact tests and in the FEM this was assumed to be clamped.
2) The workpiece was bolted to the milling machine during the impact test and it was assumed that the natural frequencies of the machine are very high compared to that of the workpiece, hence their influence can be ignored in the FEM analysis.
3) The mass of the accelerometer was assumed to be a point mass added to the FEM model.

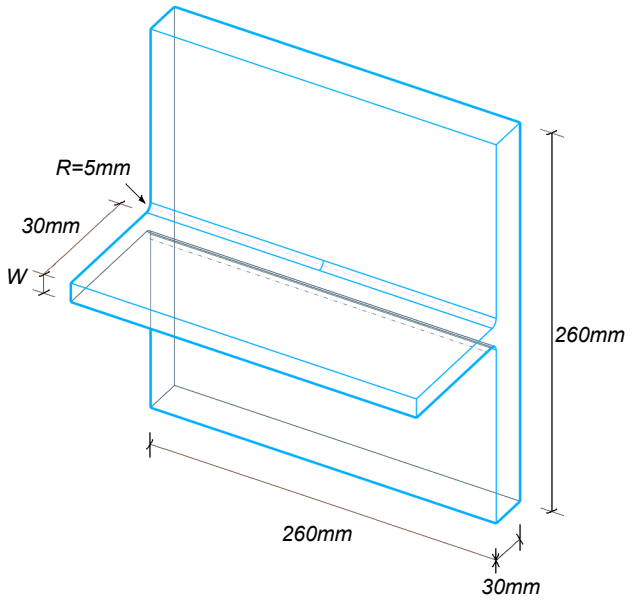

Figure 2 – Workpiece dimensions.

A. The Damping Ratio

The damping ratios, ζ_p used in (19) here for demonstrating the proposed approach were identified through impact tests (given in tables 1, 2 and 3). Adetoro et al. [35, 36] however recently proposed an approach to predicting the damping parameters for different wall thicknesses during machining of thin wall sections. This approach can be adapted with the FEM approach proposed in this paper as shown in [36] to form a unified model that would not require further experiments carried out for different wall thicknesses.

In the experimental impact tests, the workpiece is excited using an instrumented hammer, whilst the accelerometer is placed on the opposite side of the impact point, to measure the direct transfer function. Using a Fourier analyser, the accelerance frequency response function is extracted for each impact test. This is simply the division of the Fourier transform of the measured time domain input force $f(t)$ and acceleration $\ddot{x}(t)$.

$$Acc(\omega) = \frac{\ddot{X}(\omega)}{F(\omega)}, \tag{27}$$

where $Acc(\omega)$ is the accelerance FRF, $\ddot{X}(\omega)$ is the output acceleration signal in frequency domain and $F(\omega)$ is the input force signal in frequency domain. The experimental measurements are analysed using a modal analysis system (CutPro was used for the solutions in this paper), which scans the measured transfer function and fits a curve to the data in order to obtain the numerical values of natural frequency, damping [34].

Table 1 – Workpiece A, *W = 1.5mm*

Mode Number	Natural Frequency, ω_n (Hz)	Damping Ratio, ζ_p (%)
1	1323.00	2.9345E-02
2	1604.00	2.6765E-03
3	1708.00	1.9422E-03
4	1908.00	2.2348E-03
5	2196.00	1.4750E-03
6	2566.00	1.6500E-03
7	3021.00	2.0739E-03
8	3571.215	8.0504E-03

Table 2 – Workpiece B, *W = 3.0mm*

Mode Number	Natural Frequency, ω_n (Hz)	Damping Ratio, ζ_p (%)
1	2830.5000	2.5449E-02
2	3204.5000	4.4995E-03
3	3406.0000	2.9076E-03
4	3798.0000	4.8137E-03
5	4372.0000	5.3524E-03

Table 3 – Workpiece C, *W = 4.5mm*

Mode Number,	Natural Frequency, ω_n (Hz)	Damping Ratio, ζ_p (%)
1	4253.0000	3.4222E-02
2	4568.0000	9.0496E-03
3	4894.0000	8.2851E-03

V. Results

A. Extracting the Workpiece Transfer Function.

For workpiece A, the measured input force from the

impact test was used as the input force (in time domain) in the FEM modal analysis. The predicted acceleration (time domain) is shown in comparison to the experimental acceleration from the accelerometer (during the impact test) in Figure 3. The predicted FRF (using the approach in section 2) and experimental FRF, are compared in Figures 4 a and b respectively. The agreement between the experimental results and the predictions is satisfactory.

For workpiece B, the input force (in time domain) used in the FEM modal analysis was a Dirac delta function. The predicted and experimental FRFs are compared in Figures 5 a and b.

The agreement between the experimental results and the predictions is satisfactory.

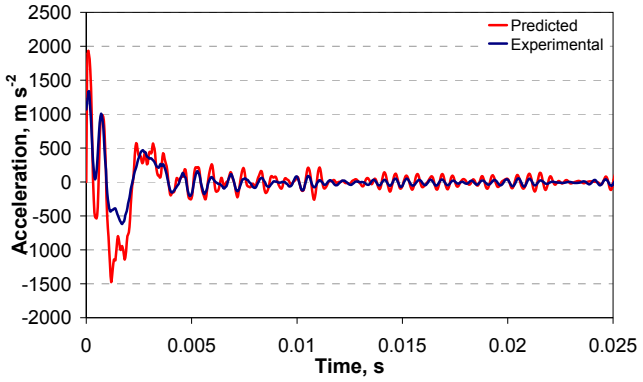

Figure 3 – Predicted and measured acceleration for workpiece A.

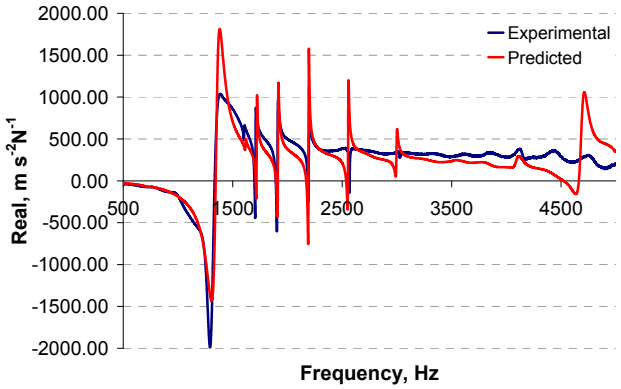

(a) Real

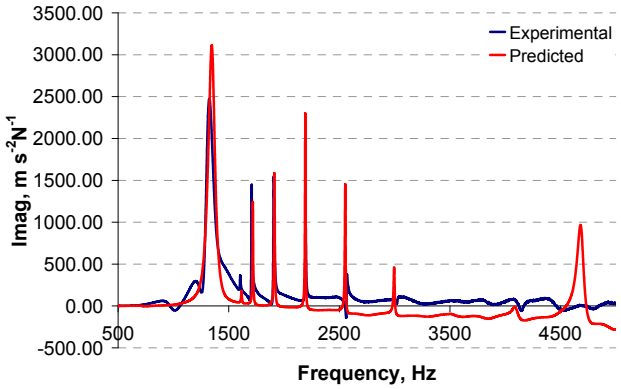

(b) Imag

Figure 4 – Predicted and measured FRFs for workpiece A, $G_{w_{yy}}$.

Figure 6 compares the predicted and experimental FRFs for workpiece C and the agreement has shown to be good.

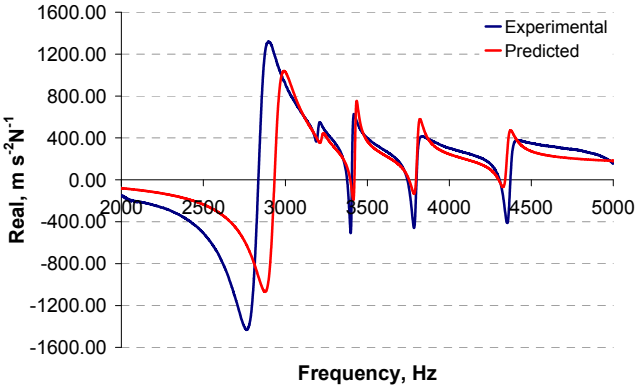

(a) Real

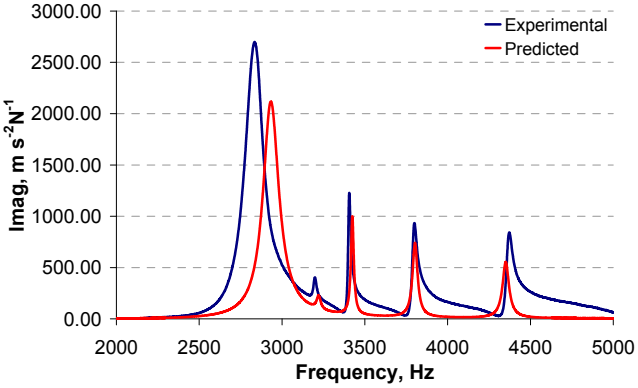

(b) Imag

Figure 5 – Predicted and measured FRFs for workpiece B, $G_{w_{yy}}$.

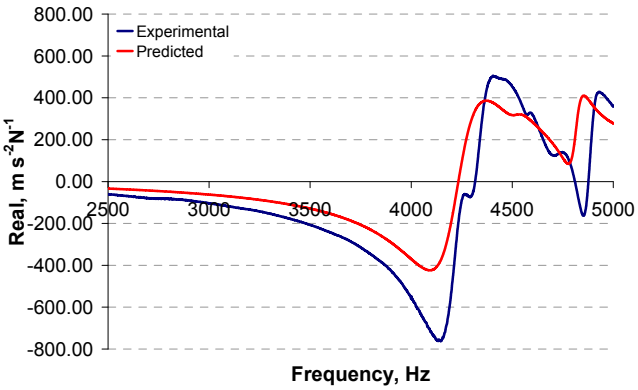

(a) Real

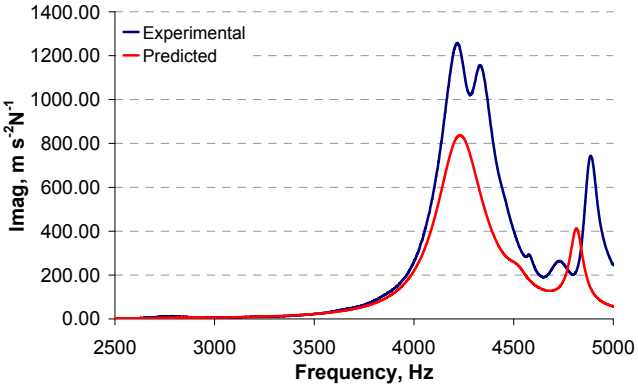

(b) Imag

Figure 6 – Predicted and measured FRFs for workpiece C, $G_{w_{yy}}$.

B. Chatter Stability Lobes.

Using both the predicted and experimental FRFs, the stability lobes were generated using CutPro, for the different types of workpiece using the parameters listed in table 4. CutPro is an advanced analytical and time-domain machining process simulation commercial package developed by Altintas. It has an in built modal analysis module and also a stability lobes module. The stability lobes module can take the transfer function in all three orthogonal directions for the workpiece and transfer function in x, and y directions for the tool.

The cutting conditions used during the simulations are detailed in table 4. The tangential cutting force coefficient (TCFC) K_t and the radial cutting constant K_r are given in this table. The radial cutting constant is a ratio of the radial cutting force coefficient to the tangential cutting force coefficient. The TCFC and the radial cutting constant are used in (5) to model the tangential and radial cutting forces respectively. The radial depth of cut or radial immersion is also given in table 4, which is used to calculate the entry and exit angles of the cutter. The entry and exit angles are used as the limits for the elements in the radial immersion dependent matrix, $[A_0]$ required when calculating the oriented transfer function $[G_0]$ in (12). The elements of the matrix $[A_0]$ are detailed in [20, 21, 22 and 24].

The predicted and experimental results are compared in Figures 7a, b & c for the three different workpiece. The comparisons show a satisfactory agreement. The slight discrepancy in the predicted natural frequency (frequency at which FRF real is zero and imaginary is maximum) can be seen in the slight shift in the spindle speed calculated in the stability lobes.

The natural frequency predicted affects the stable tooth passing frequency calculated in the stability lobes, hence the slight differences seen in the spindle speeds. The predicted stable axial depth of cuts in Figures 7 b and c are slightly higher than the experimental stable ADOC and this is due to the FEM model being too stiff. This can be caused by the boundary condition assumption stated in section 3, where the back surface was assumed to be perfectly clamped. In the FEM stiffness matrix formulation, the elements are therefore set to 1E+36 and the degrees of freedom at this surface are not included in the simulation. A more accurate approach would require knowledge of the friction at the boundary between the machine and the workpiece.

Table 4 – Cutting Condition and Coefficients

	WORKPIECE A	WORKPIECE B	WORKPIECE C
K_R	-0.7040	0.3030	1.1459
K_T (MPA)	981.6966	801.0970	679.6021
RADIAL DEPTH OF CUT, (mm)	0.500	1.000	2.000

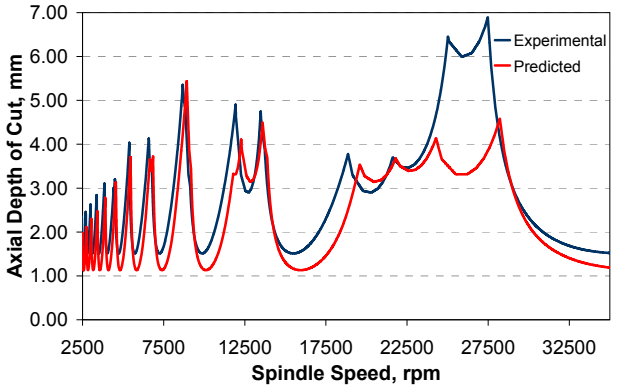

(a) Workpiece A

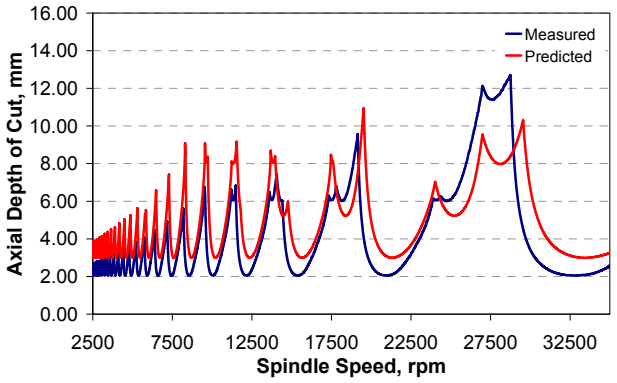

(b) Workpiece B

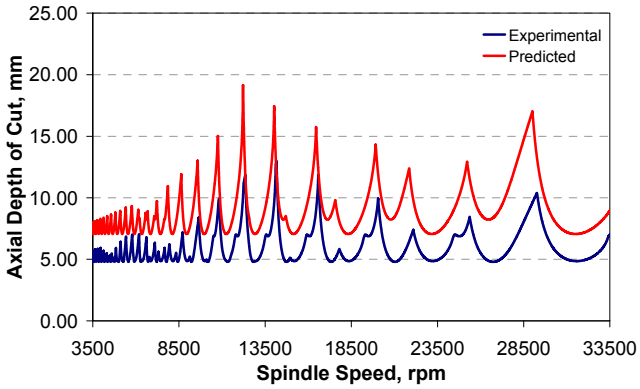

(b) Workpiece C

Figure 7 – Stability lobes comparison.

C. Experimental Results

To show the advantages of this approach in thin-wall machining, a typical surface finish obtained for a thin walled section is shown in Figure 9. and the cutting forces shown in Figure 8. This experimental results show that the varying dynamics along the workpiece cannot be ignored or assumed as constant. In the surface finish it is shown that the workpiece is unstable only at the end of the cut, while this is confirmed in the cutting force (F_x) plot. These results are shown and discussed in-depth in [30]. Therefore using the approach in this paper, the transfer function along the workpiece can be easily extracted without reliance on experimental results.

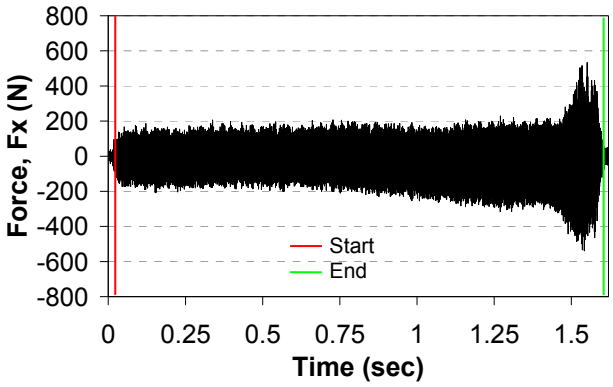

Figure 8 – Experimental cutting forces from [30].

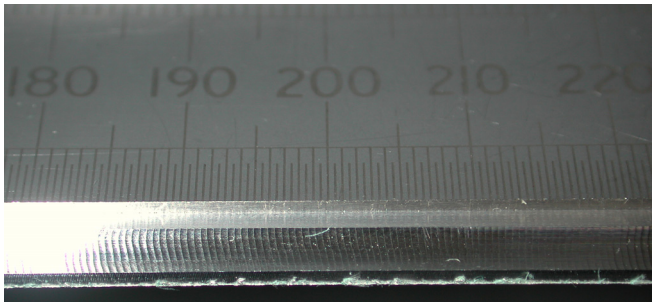

(a) – Part I

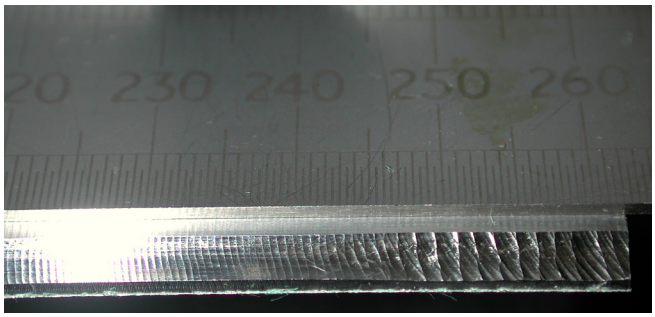

(b) – Part II

Figure 9 – Surface finish thin wall machining [30].

For completeness, the full FRF matrix in (11) is also required, however applying the impact force and/or measuring the response in certain directions experimentally can prove difficult. Using the proposed approach however, the full FRF matrix in (11) can be obtained easily in all directions. This is done by simply applying the impact force in the corresponding directions of interest.

VI. Conclusion

Chatter still undermines the efforts of the machinist by reducing surface quality, productivity and increasing cost in damage repair. In this paper, an alternative approach to extracting the transfer function using the FEM modal analysis has been presented. The approach is based on the Fourier transform of the results obtained from the finite element analysis. The results are shown to agree with experimental results and hence the transfer function calculated. Its accuracy is further explored by its use in stability lobe predictions. This approach can be used to solve different problems encountered through the use of impact test, including obtaining the frequency response function in directions that ca prove difficult experimentally.

Acknowledgements

The authors acknowledge the support given by EPSRC for funding this project and also the immense support given by Airbus along with Mr. Alister Reynish (GKN Aerospace).

Reference

[1] F. W. Taylor, On the art of cutting metals, Transactions of the American Society of Mechanical Engineers, 28, (1907), pp. 31–350.
[2] S. A. Tobias and W. Fishwick, A Theory of Regenerative Chatter, The Engineer London, (1958).
[3] J. Tlusty, M. Polacek, The stability of machine tools against self excited vibrations in machining, in: Proceedings of the ASME International Research in Production Engineering, Pittsburgh, USA, (1963), pp. 465–474.
[4] F. Koenigsberger and J. Tlusty, Machine Tool Structures Stability Against Chatter, Pergamon Press, 1, (1967).
[5] H. E. Merritt, Theory of Self-Excited Machine Tool Chatter, Journal of Engineering for Industry, Transactions of the ASME, 87, (1965), pp.447 – 454.
[6] J. Tlusty and P. Ismail, Basic Nonlinearity in Machining Chatter, Annals of the CIRP, 10 (1), (1981).
[7] J. Tlusty and P. Ismail, Special Aspects of Chatter in Milling, Journal of Vibration, Acoustics, Stress, and Reliability in Design, 105, (1983).
[8] J. Slavicek, The Effect of Irregular Tooth Pitch on Stability of Milling, 6th MTDR Conference Manchester, (1965).
[9] P. Vanherck, Increasing Milling Machine Productivity by Use of Cutters with Non-Constant Cutting – Edge Pitch, 8th MTDR Conference Manchester, (1967).
[10] R Sridhar, R. E. Hohn and G. W. Long, General Formulation of the Milling Process Equation, Journal of Engineering for Industry, Transactions of the ASME, (1968), pp. 317 – 324.
[11] R. Sridhar, R.E. Hohn, and G.W. Long. A Stability Algorithm for the General Milling Process, Journal of Engineering for Industry, Transactions of the ASME, (1968), pp. 330 – 334.
[12] R.E. Hohn, R. Sridhar, and G.W. Long. A Stability Algorithm for a Special Case of the Milling Process, Journal of Engineering for Industry, Transactions of the ASME, (1968), pp. 325 – 329.
[13] H. Opitz, Chatter Behaviour of Heavy Machine Tools, Quarterly Technical Report No. 2 AF 61 (052) – 916 Research and Technology Division Wright Patterson Air Force Base OH. (1968).
[14] H. Opitz and F. Bernardi, Investigation and Calculation of the Chatter Behaviour of Lathes and Milling Machines, Annals of the CIRP, 18, (1970), pp. 335 – 343.
[15] J. Tlusty and F. Koenigsberger, Machine Tool Structures, Pergamon Press Oxford 5th Edn., 1, (1970).
[16] I. Minis, T. Yanushevsky, R. Tembo and R. Hocken, Analysis of Linear and Nonlinear Chatter in Milling, Annals of the CIRP, 39, (1990), pp. 459 – 462.
[17] I. Minis and T. Yanushevsky, A New Theoretical Approach for the Prediction of Machine Tool Chatter in Milling, Journal of Engineering for Industry, Transactions of the ASME, 115, (1993), pp. 1-8.
[18] A. C. Lee and C. S. Liu, Analysis of Chatter Vibration in the End Milling Process, International Journal of Machine Tool Design and Research, 31(4), (1991), pp. 471 – 479.
[19] A. C. Lee, C. S. Liu and S. T. Chiang, Analysis of Chatter Vibration in a Cutter – Workpiece System, International Journal of Machine Tool Design and Research, 31(2), (1991), pp. 221 – 234.
[20] E. Budak, Mechanics and dynamics of milling thin walled structures. Ph.D. Thesis, The University of British Columbia, Vancouver, B.C., Canada, (1994).
[21] Y. Altintas and E. Budak, Analytical prediction of stability lobes in milling, CIRP Annals - Manufacturing Technology, 44(1), (1995), pp. 357 – 362.
[22] E. Budak and Y. Altintas, Analytical prediction of chatter stability in milling - Part I: General formulation, Proceeding of ASME 1995 International Mechanical Engineering Conference and Exposition, San Francisco, USA, (1995).
[23] E. Budak, Analytical Prediction of Chatter Stability in Milling – Part I: General Formulation, Journal of Dynamic Systems, Measurement and Control, Transactions of the ASME, 120, (1998), pp. 22 – 30.
[24] Y. Altintas, E. Shamoto, P. Lee and E. Budak, Analytical Prediction of Stability Lobes in Ball-End-Milling, Journal of Manufacturing Science and Engineering Transactions of the ASME, 121(4), (1999), pp. 586 – 592.

[25] Y. Altintas, Analytical prediction of three dimensional chatter stability in milling, JSME International Journal, Series C: Mechanical Systems, Machine Elements and Manufacturing, 44(3), (2001), pp. 717-723.
[26] F. J. Campa, L. N. Lopez de Lacalle, A. Lamikiz and J. A. Sanchez, Selection of cutting conditions for a stable milling of flexible parts with bull-nose end mills, Journal of Materials Processing Technology, 191(1-3), (2007), pp. 279 – 282.
[27] O. B. Adetoro, W. M. Sim, and P. H. Wen, Stability Lobes Prediction for Corner Radius End Mill using Nonlinear Cutting Force Coefficients, Machining Science and Technology (submitted for publication – August 2009).
[28] V. Thevenot, L. Arnaud, G. Dessein and G. Cazenave-Larroche, Influence of Material Removal on the Dynamics Behavior of Thin-walled Structures in Peripheral Milling. Machining Science and Technology, 10, (2006), pp. 275 – 287.
[29] S. Seguy, F. J. Campa, L. N. Lopez de Lacalle, Toolpath dependent stability lobes for the milling of thin-walled parts, International Journal of Machining and Machinability of Materials, 4(4), (2008), pp. 377 – 392.
[30] O. B. Adetoro, W. M. Sim, and P. H. Wen, Accurate Prediction of Stability Lobes using Nonlinear Thin Wall Dynamics, Journal of Material Processing Technology, (submitted for publication – August 2009).
[31] R. G. Grimes, J. G. Lewis and H. D. Simon, A Shifted Block Lanczos Algorithm for Solving Sparse Symmetric Generalized Eigenproblems, SIAM Journal on Matrix Analysis and Applications, 15, (1994), pp. 228 – 272.
[32] Karlsson & Sorensen, Inc. Hibbitt, Abaqus Theory Manual, 1080 Main Street Pawtucket Rl 02860 – 4847 USA, (2006).
[33] S. W. Smith, The Scientit & Engineer's Guide to Digital Signal Processing, California Technical Pub. San Diego, 1st edition, (1997). Available: http://www.dspguide.com.
[34] Y. Altintas, Manufacturing Automation, Cambridge University Press, New York, NY (2000).
[35] O. B. Adetoro, W. M. Sim, P. H. Wen, R. Vepa, Prediction of Proportional Damping Parameters, Journal of Advanced Manufacturing Systems, (submitted for publication – April 2009).
[36] O. B. Adetoro, W. M. Sim, P. H. Wen, A New Damping Modelling Approach and its Application in Thin Wall Machining, The International Journal of Advanced Manufacturing Technology (submitted publication – May 2009).